A COMPARISON STUDY ON TRANSITION CHARACTERISTICS OF NLF FORWARD-SWEPT-WING AND AFT-SWEPT-WING

Zhen Zhu, Wen-Ping Song, Zhong-Hua Han, Jian-Hua Xu
National Key Laboratory of Science and Technology on Aerodynamic Design and Research, Northwestern Polytechnical University, Xi'an, 710072, P. R. China

Keywords: *transition prediction, e^N method, natural laminar flow, forward-swept wing, cross flow instability*

Abstract

The forward-swept-wing (FSW) is a favorable concept in natural laminar flow (NLF) wing design. It has smaller leading edge swept angle λ_{LE} than that of aft-swept-wing (ASW), which may avoid leading edge transition induced by cross flow (CF) instability. However, there are still some key technological issues, such as the characteristics of boundary layer transition in transonic flow, aerodynamic performances and the differences of CF instability between FSW and ASW, are not clear. A comparison study on transition characteristics, boundary layer stability and aerodynamic performances of NLF FSW and ASW is carried out. A three-dimensional Reynolds-averaged Navier-Stokes (RANS) solver coupled with a dual e^N transition prediction method based on linear stability theory (LST) is used. Fixed wave angle method and fixed wave number method are employed for Tollmien-Schlichting (TS) instability and cross-flow instability, respectively. The results show that, 1). With the same λ_{LE}, the FSW in this paper has a smaller CF instability and larger area of laminar flow than that of ASW. 2). Compared with ASW, the FSW has larger swept angle at about 50%-60% chord where shock wave may occur, which leads to much weaker shock wave. 3). C_L/C_D of the FSW is 13.7% larger than that of ASW. It can be concluded that FSW has more advantages in NLF supercritical wing design.

1 Introduction

With the consideration of fuel conservation and environmentally friendly obligation, drag reduction is one of the most important issues in the design of next generation civil transport aircraft. For civil transport aircraft in high subsonic flight, the skin-friction drag can account for almost 50% of the total drag[1]. The skin-friction drag of laminar boundary layer is much smaller than that of turbulent boundary layer at the same Reynolds number. Therefore, NLF wing technology can effectively reduce friction drag by maintaining a large range of laminar flow on the surface of wing. Although NLF wing technology is considered as one of the most potential technologies of drag reduction, and has been applied to unswept wing, difficulty still exists for its implement in aft-swept-wing because of cross-flow instability.

ASW with leading edge sweep angle greater than 25° is generally used in modern civil transport aircraft, to delay shock wave and get higher cruising speed. The boundary layer transition onset of swept wing can be caused by not only Tollmien-Schlichting (TS) waves but also CF instability (CFI). The amplification of TS wave disturbances can be depressed by extending the range of favorable pressure gradient, which is how NLF airfoil works. However, in contrast with the TS instability (TSI), CF instability disturbances amplify fast in favorable pressure gradient region and often induce transition onset at leading edge. Therefore, a smaller swept angle is required to reduce skin-friction drag by weakening CF instability, and a larger swept angle is required

to reduce shock wave drag at higher cruising speed. So, how to achieve the purpose of overall drag reduction by maintaining a large range of laminar flow at high cruise speed becomes a difficult problem of civil aircraft NLF wing design.

Forward-swept wing layout is a favorable concept for NLF wing design[2]. As an inevitable obstacle of the wide application of FSW, aeroelastic divergence property can be improved with the development of advanced composite materials and aeroelastic tailoring design. FSW has a great potential to become the advanced aircraft layout of next generation. However, the mechanism of boundary layer transition characteristics of NLF FSW in high subsonic flight, and the difference of CF instability between FSW and ASW are still not fully understood.

In this paper, a comparison study on transition characteristics of FSW and ASW is carried out. A dual e^N method based on linear stability theory for the prediction of transition induced by TS waves and CF instability is coupled with a three-dimensional RANS solver, PMNS3D[3].

2 Aerodynamic Analysis Method

2.1 e^N Transition Prediction Method

Accurate and reliable prediction of boundary layer transition onset from laminar to turbulent flow is one of the key issues for NLF FSW transition characteristics study. In this paper, transition location is predicted automatically by e^N method coupled with a RANS solver, PMNS3D[3]. Based on linear stability theory, the e^N method can also offer the instability characteristics for transition mechanism study.

We assume that the small disturbance is a sinusoidal wave, so the expression of three-dimensional small disturbance q' based on the parallel flow approximation and spatial amplification theory is

$$q'(x,y,z,t)=\hat{q}(y)e^{-(\alpha_i x+\beta_i z)}e^{i(\alpha_r x+\beta_r z-\omega t)}, \quad (1)$$

where q' is the small disturbance of any flow variable q, and x, y, z are the directions of the non-orthogonal body-fitted coordinate, respectively, t represents time. $\hat{q}$ is the amplitude function of small disturbance. The parameters α_i and β_i denote the spatial amplification rates in x- and z-directions, α_r and β_r denote the wave numbers in x- and z-directions, and ω is the dimensionless radian frequency.

Then small disturbances in boundary layer flow are analysed with LST. If all the small disturbances are decayed, the boundary layer flow is stable. Oppositely, if some of the small disturbances are amplified, the boundary layer flow is unstable. For the unstable disturbance, compared with the amplitude of disturbance at the location where it begins to be amplified, the location where the amplitude is amplified by a factor of e^N times is viewed as the transition onset location.

For swept wings, the boundary layer transition can be induced by not only TSI, but also CFI, therefore, a dual e^N method based on LST is adopted to predict transition of FSW and BSW boundary lays in this paper. Two N factors, N_{TS} and N_{CF}, are calculated simultaneously with different integration strategies, which will be talked about in details in Section 2.1.1 and Section 2.1.2, where N_{TS} is for TSI and N_{CF} is for CFI.

2.1.1 Fixed Wave Angle Method

For TS instability, N_{TS}, i.e., N factor of TSI is calculated by fixed wave angle method instead of envelope method:

$$N_{TS}=\max_{f,\psi=0}\int_{x_0}^{x}-\alpha_i dx, \quad (2)$$

where N_{TS} is the integral of disturbance amplification rates of TSI; f denotes the dimensional frequency of TS wave; ψ denotes the angle between wave number vector of disturbance wave and x-axis, which is also defined as wave angle; and x_0 corresponds to the x-location where disturbance begin to be amplified. It can be seen that wave angle $\psi = 0°$, which means the the direction of the inviscid flow at the boundary layer outer edge is selected

as the propagation direction of disturbance waves with different frequencies. By this way, it can be ensured that none of CFI disturbances will be mixed into N_{TS}, so only TSI disturbance amplification rates are integrated.

2.1.2 Fixed Wave Number Method

As to CF instability, N_{CF}, i.e., N factor of CFI is calculated using fixed wave number method in this paper:

$$N_{CF} = \max_{\beta_r, f=0} \int_{x_0}^{x} -\alpha_i dx \,, \qquad (3)$$

where N_{CF} is the integral of disturbance amplification rates of CFI; β_r is the wave number in z-direction, which de-notes the span-wise wave number of CF wave here; f is the dimensional frequency of CF wave, so f = 0Hz means stationary CF wave. For the low-turbulence environment representative for the realistic flight environment of a modern transport aircraft, the stationary CF waves play a more important role than the travelling waves. Thus, it is reasonable to only consider stationary CF waves.

2.1.3 Dual e^N Transition Prediction Method

In this paper, e^N method using dual N factors, N_{TS} and N_{CF}, for transition caused by both TSI and CFI is employed. The dual e^N method is a framework of transition prediction method, two different integration strategies of N factors for the integral of disturbance amplification rates of TSI and CFI are selected properly. In this paper, wave angle method is adopted for N_{TS}, and wave number method is adopted for N_{CF}. According to the thresholds $[(N_{TS})_{tr}, (N_{CF})_{tr}]$, the transition location x_{tr} of boundary layer flow over swept-wing can be obtained. If N_{TS} reaches its corresponding threshold $(N_{TS})_{tr}$ firstly, the boundary layer flow transition is considered to be dominated by TSI at x_{TS}. In contrast, if N_{CF} reaches $(N_{CF})_{tr}$ firstly, the transition caused by CFI is considered to occur at x_{CF}.

2.2 Coupling Process of RANS Solver and Dual e^N Transition Prediction Method

As mentioned above, A dual e^N method fully solving linear stability equations with two different strategies is employed to predict the location of transition induced by TSI and CFI simultaneously. The transition prediction module is coupled to the RANS solver towards automatic transition prediction. The coupling of the RANS solver and the module of transition prediction is sketched in Fig. 1. The pressure coefficients at the outer edge of the boundary layer from RANS solver are used as the inputs for the boundary-layer solver, which in turn outputs the velocity profiles, temperature profiles and their first- and second-order derivatives necessary for linear stability analysis. After the linear stability equations are solved, the aforementioned dual e^N method is used to calculate the amplification of both TS and CF waves. Then, the transition locations are fed back to the RANS solver. This process is repeated until both transition lines and the residual of the RANS equations are converged.

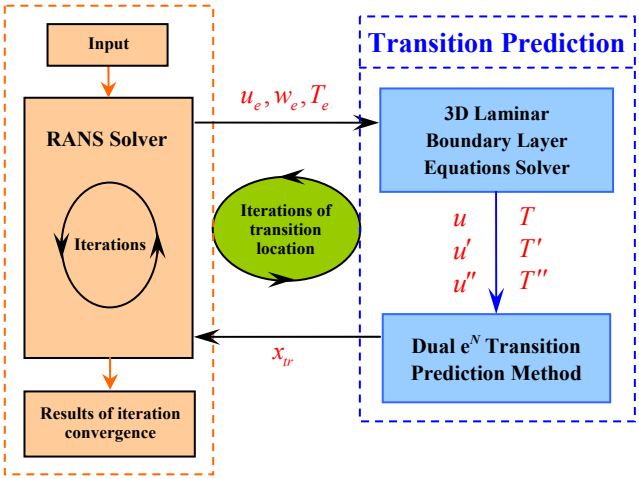

Fig. 1: Coupling process of RANS solver and e^N Transition prediction method

2.3 Method Validation

Validation of dual e^N method are carried out by two infinite swept-wing cases. There is no difference between FSW and ASW when they are both infinite. The test cases are the transition predictions of flows over infinite swept-wings with a NACA64$_2$A015 airfoil mounted normal to the leading edge. The swept angles λ are 10º and 40º. The experimental data is from the Ames 12-Foot Low-Turbulence Pressure

Tunnel[4]. Simulations of flows over the infinite swept-wings are carried out using C-H structured grids with size as 353×105×9. For the 10° swept wing, the computations are performed at Mach number, Ma = 0.27. Reynolds number, Re ranges from 5×10^6 to 2.5×10^7. Angle of attack α is fixed at 0.0°. For the 40° swept wing, the computations are also performed at Ma = 0.27, Re ranges from 4.6×10^6 to 7.3×10^6, angle of attack α is fixed at -1.5°. The thresholds of N_{TS} factor and N_{CF} factor, $[(N_{TS})_{tr}, (N_{CF})_{tr}]$ are set as [10.5, 7.5] based on the experience.

For the 10° swept wing, comparisons between the calculated transition locations on the upper surfaces of wing and experiments are shown in Fig. 2, It can be seen that the transition locations calculated by dual e^N method are in good agreement with experimental results. For a wing with small swept angle(10°), the transition should be dominated by TS instability, and this transition mechanism can also be given by dual e^N method. Fig. 3 shows the N factors of TSI and CFI on the upper surfaces of wing at Re of 4.6×10^6.

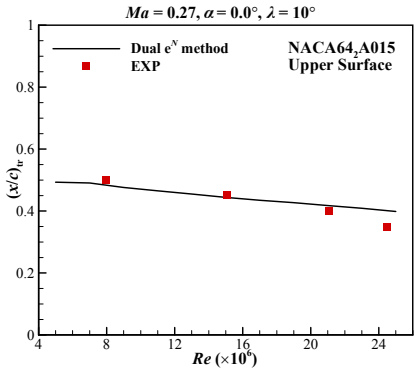

Fig. 2: Transition locations on upper surface of 10° swept NACA64$_2$A015 wing

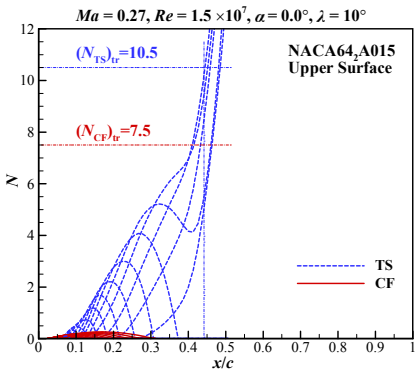

Fig. 3: N factors of TSI and CFI on upper surface of 10° swept NACA64$_2$A015 wing

According to the N factors curves, we can see that unstable TSI disturbances begin to be amplified after leading edge acceleration zone. Compared to CFI disturbances, TSI disturbances are amplified very quickly and finally reach $(N_{TS})_{tr}$, i.e., 10.5 earlier, which means the onset of transition caused by TSI is assumed to happen.

For another wing with larger swept angle (40°), the transition is dominated by CF instability. Transition locations on the upper surfaces of wing calculated by dual e^N method is in good agreement with experimental results, which can be seen in Fig. 4. The N factors of TSI and CFI on the upper surfaces of wing at Re of 6.3×10^6 are shown in Fig. 5.

According to the N factors curves, we can see that unstable CFI disturbances begin to be amplified just from the very beginning of leading edge. CFI disturbances of 40° swept wing are amplified much more sharply than that of 10° swept wing in the whole acceleration zone. N factors of CFI disturbances grow faster than that of TSI disturbances, and reach $(N_{CF})_{tr}$,

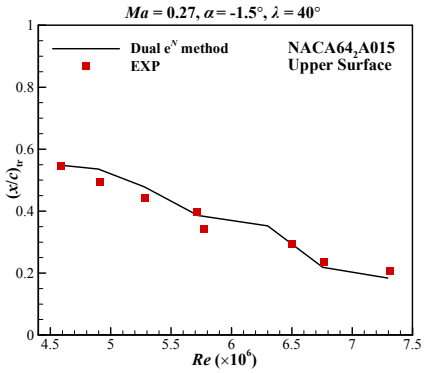

Fig. 4: Transition locations on upper surface of 40° swept NACA64$_2$A015 wing

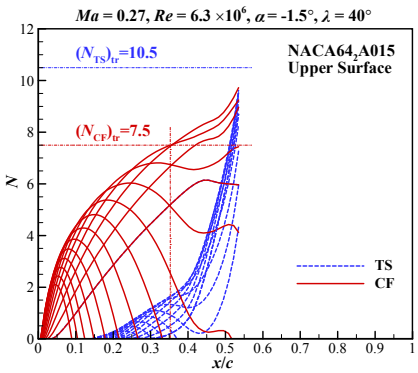

Fig. 5: N factors of TSI and CFI on upper surface of 40° swept NACA64$_2$A015 wing

i.e., 7.5 first. Obviously, transition onset is caused by strong CF instability of large leading edge swept angle. Through the above two test cases, it can be proved that dual e^N method can not only predict quiet reliable transition locations, but also give the right transition mechanism.

3 Transition Characteristics of NLF FSW and ASW

Transition prediction of a FSW is carried out with the method mentioned above. The aspect ratio is 10.5, the taper ratio is 0.3, and the leading edge sweep angle is 25°. Both tip section and root section are NLF supercritical airfoil NPU-LSC-72613[5]. No geometric twist is taken. The C-H structured grid with size as 233×105×49 is used for simulating the flow around the FSW. The *Re* based on the wing mean aerodynamic chord is 2.0×10^7, the *Ma* is 0.78 and the lift coefficient, C_L is 0.5 (error ± 0.5%). Spalart-Allmaras turbulence model is applied to simulate turbulent flow. the transition critical *N* factors [$(N_{TS})_{tr}$, $(N_{CF})_{tr}$] are set as [10.5, 7.5] based on the experience. Pressure coefficients and transition lines on both upper and lower surfaces are shown in Fig. 6.

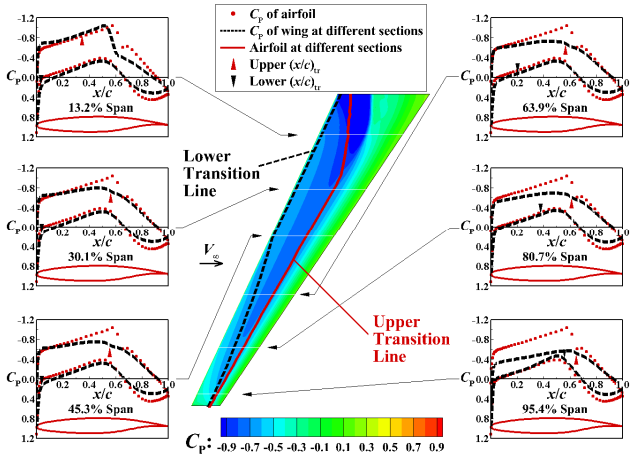

Fig. 6: Pressure coefficients and transition lines of FSW

In the figures of pressure distributions of different stations, the black lines are pressure distributions at local station of the wing and the red dots are pressure distribution of NPU-LSC-72613 airfoil in the design condition. The red solid line are the transition lines on upper surfaces and the black dashed line is transition line on lower surfaces. The pressure distributions show that FSW has no shock wave except the station near wing root， because of quiet large swept angle at about 50%-60% chord, where shock wave may occur. The transition lines show that much larger S_{lam} (area of laminar flow zone/wetted area) on the upper surface (48.3%) than S_{lam} on lower surface (13.3%). The reason is CFI on lower surface are stronger than that on upper surface and causes earlier transition onset, especially leading edge transition on inner-board stations, which can be seen in Fig. 7.

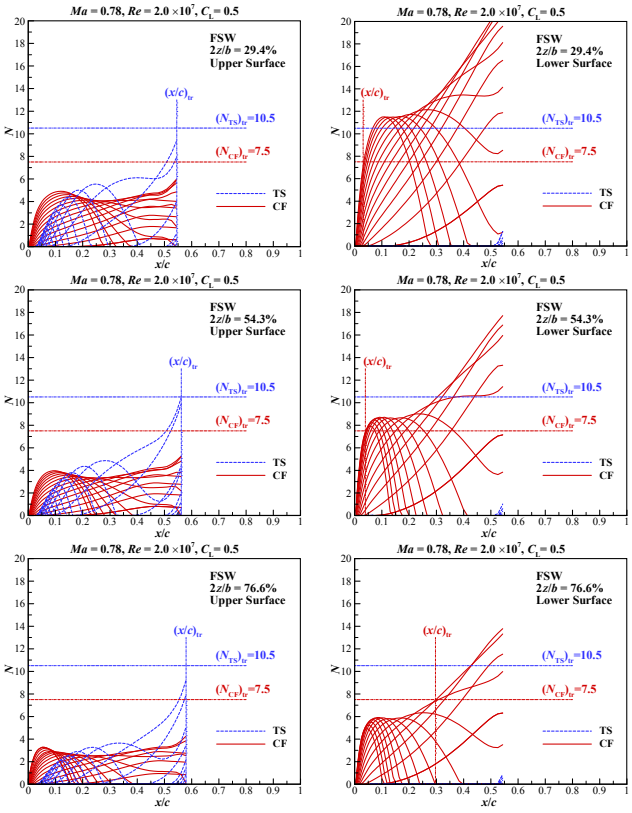

Fig. 7: *N* factors of TSI and CFI at different spanwise stations of FSW

To make a comparison with the transition characteristics of the FSW, transition prediction of an ASW with the same aspect ratio (10.5), taper ratio (0.3), Λ_{LE} (25°), tip section and root section (NPU-LSC-72613), is carried out in the same *Re* (2.0×10^7), *Ma* (0.78)and C_L (0.5 error ± 0.5%). Pressure coefficients and transition lines on both upper and lower surfaces of the ASW are shown in Fig. 8. The pressure distributions show that ASW has a strong shock wave except

the station near wing tip， because of smaller swept angle at about 50%-60% chord. The transition lines on upper surface and lower surface of ASW show some quiet similar characteristics with that of FSW, which are larger area of laminar flow on the upper surface (39.1%) and smaller on lower surface (12.0%) caused by earlier transition onset, or even leading edge transition on inner-board stations. We can also see that both of the laminar flow areas on upper and lower surfaces are smaller than that of FSW.

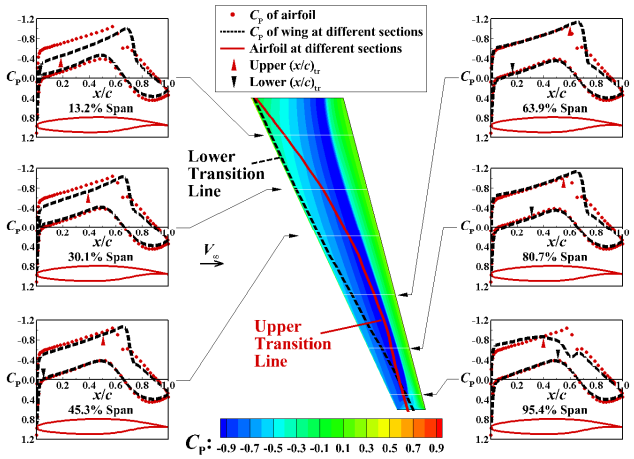

Fig. 8: Pressure coefficients and transition lines of ASW

To take a closer look at the differences of transition characteristics, boundary layer cross-flow stability and performances of NLF FSW and ASW, comparison of transition lines and N_{CF} factors between FSW and ASW are shown in Fig. 9 and comparison of aerodynamic performances and S_{lam} in Tab. 1. It can be seen in Fig. 9 that, because of three-dimensional displacement effect, even though with the same λ_{LE}, FSW has smaller CF instability and later transition onset locations compared with ASW at most of the stations of wing. This leads to 20.5% larger range of laminar flow area of FSW than that of ASW shown in Tab. 1. As mentioned before, ASW has a much stronger shock wave compared with BSW. Take these two points into consideration, the result that FSW layout has 13.7% larger C_L/C_D than ASW can be explained.

Tab. 1: Comparison of aerodynamic performances and S_{lam} of FSW and ASW

		ASW	FSW	$\triangle_{(FSW-ASW)/ASW}$
C_L		0.500	0.502	/
C_D		0.0176	0.0155	-11.5%
C_L/C_D		28.4	32.3	+13.7%
S_{lam}	Upper	39.1%	48.3%	+23.4%
	Lower	12.0%	13.3%	+11.1%
	Total	25.5%	30.8%	+20.5%

4 Conclusions

A comparison study on transition characteristics, boundary layer stability and aerodynamic performances of a NLF FSW and a ASW with the same λ_{LE} (25°) is carried out in this paper. The results show that:

1). The FSW has a smaller CF instability and 20.5% larger area of laminar flow than that of ASW. Because the three-dimensional displacement effects of wings are pushing flow along the direction from root to tip, which is opposite to the cross flow direction of FSW.

2). Compared with ASW which has the same λ_{LE}, the FSW has larger swept angle at about 50%-60% chord where shock wave may occur, which leads to much weaker shock wave.

3). It can be concluded that, FSW has more advantages in NLF supercritical wing design, such as larger laminar flow area and much weaker shock wave. C_L/C_D of the FSW in this paper is 13.7% larger than that of ASW.

Acknowledgements

This work was supported by the Aeronautical Science Foundation of China (2016ZA53) and the ATCFD Project(2015-F-016).

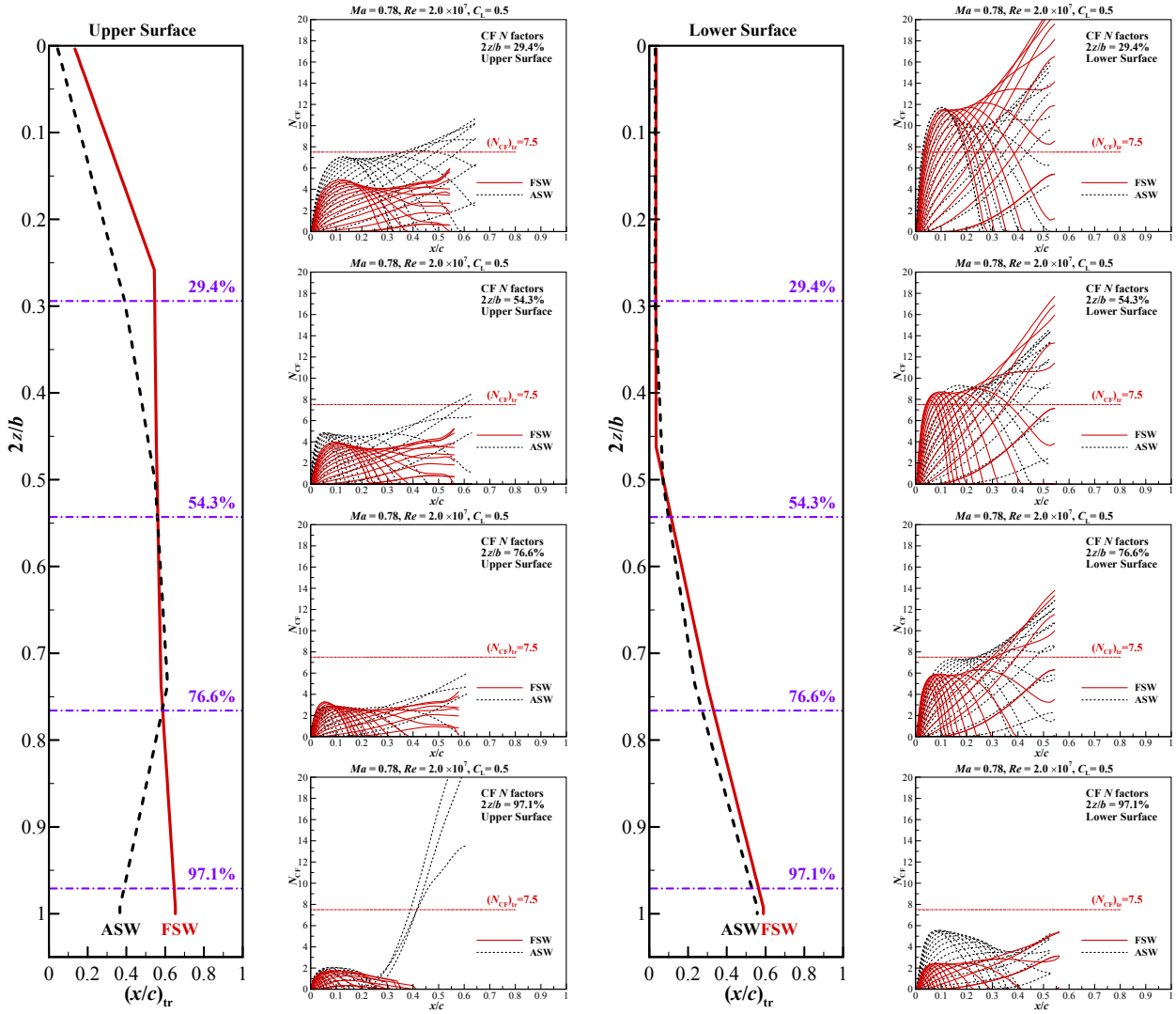

(a) Upper surface (b) Lower surface

Fig. 9: Comparison of transition lines and N_{CF} factors between FSW and ASW with the same $\lambda_{LE} = 25°$

References

[1] Reneaux J, Thibert J J and Schmitt V. ONERA activities on drag reduction, ICAS paper, 1990: 90-3.6 (1990).

[2] Redeker G and Wichmann G. Forward sweep - A favorable concept for a laminar flow wing, Journal of Aircraft, 28(1991):97-103 (1991).

[3] Song WP, Zhu Z, Yang H, et al. Laminar flow wing's optimization design by RANS solver with automatic transition prediction[C]//28th Congress of the International Council of the Aeronautical Sciences 2012, 2012: 716-725.

[4] Boltz F W, Kenyon G C and Allen C Q. Effects of sweep angle on the boundary-layer stability characteristics of an untapered wing at low speeds[R]. NASA, 1960.

[5] Han ZH, Deng J, Liu J, et al. Design of laminar supercritical airfoils based on Navier-Stokes equations[C]//28th Congress of the International Council of the Aeronautical Sciences 2012, 2012: 706-715.

Contact Author Email Address

Prof. Dr. Zhong-Hua Han
Mailto:hanzh@nwpu.edu.cn

Copyright Statement